

## Non-classical large deviations for a noisy system with non-isolated attractors

This article has been downloaded from IOPscience. Please scroll down to see the full text article.

J. Stat. Mech. (2012) P05028

(<http://iopscience.iop.org/1742-5468/2012/05/P05028>)

View [the table of contents for this issue](#), or go to the [journal homepage](#) for more

Download details:

IP Address: 140.77.78.63

The article was downloaded on 27/07/2012 at 13:05

Please note that [terms and conditions apply](#).

# Non-classical large deviations for a noisy system with non-isolated attractors

Freddy Bouchet<sup>1</sup> and Hugo Touchette<sup>2</sup>

<sup>1</sup> Laboratoire de Physique, ENS Lyon, 46 allée d'Italie, 69364 Lyon, France

<sup>2</sup> School of Mathematical Sciences, Queen Mary University of London, London E1 4NS, UK

E-mail: [Freddy.Bouchet@ens-lyon.fr](mailto:Freddy.Bouchet@ens-lyon.fr) and [H.Touchette@qmul.ac.uk](mailto:H.Touchette@qmul.ac.uk)

Received 30 April 2012

Accepted 15 May 2012

Published 31 May 2012

Online at [stacks.iop.org/JSTAT/2012/P05028](http://stacks.iop.org/JSTAT/2012/P05028)

[doi:10.1088/1742-5468/2012/05/P05028](https://doi.org/10.1088/1742-5468/2012/05/P05028)

**Abstract.** We study the large deviations of a simple noise-perturbed dynamical system having continuous sets of steady states, which mimic those found in some partial differential equations related, for example, to turbulence problems. The system is a two-dimensional nonlinear Langevin equation involving a dissipative, non-potential force, which has the essential effect of creating a line of stable fixed points (attracting line) touching a line of unstable fixed points (repelling line). Using different analytical and numerical techniques, we show that the stationary distribution of this system satisfies, in the low-noise limit, a large deviation principle containing two competing terms: (i) a ‘classical’ but sub-dominant large deviation term, which can be derived from the Freidlin–Wentzell theory of large deviations by studying the fluctuation paths or instantons of the system near the attracting line, and (ii) a dominant large deviation term, which does not follow from the Freidlin–Wentzell theory, as it is related to fluctuation paths of zero action, referred to as sub-instantons, emanating from the repelling line. We discuss the nature of these sub-instantons, and show how they arise from the connection between the attracting and repelling lines. We also discuss in a more general way how we expect these to arise in more general stochastic systems having connected sets of stable and unstable fixed points, and how they should determine the large deviation properties of these systems.

**Keywords:** stochastic processes (theory), nonlinear dynamics, large deviations in non-equilibrium systems, diffusion

**ArXiv ePrint:** [1204.6269](https://arxiv.org/abs/1204.6269)

---

**Contents**

<b>1. Introduction</b>	<b>2</b>
<b>2. Model</b>	<b>4</b>
<b>3. Path integral solution</b>	<b>6</b>
3.1. Classical theory . . . . .	6
3.2. Sub-instantons . . . . .	9
<b>4. Dynamical analysis</b>	<b>11</b>
4.1. Energy . . . . .	12
4.2. Dynamics around stable fixed points . . . . .	13
4.3. Dynamics around unstable fixed points . . . . .	14
<b>5. Hamilton–Jacobi approach</b>	<b>16</b>
5.1. Stable fixed points . . . . .	16
5.2. Unstable fixed points . . . . .	19
<b>6. Discussion</b>	<b>20</b>
<b>Acknowledgments</b>	<b>22</b>
<b>References</b>	<b>22</b>

---

**1. Introduction**

The dynamics of physical systems described by partial differential equations, such as those appearing in hydrodynamics, optics or quantum physics, are in many cases qualitatively similar to those of finite-dimensional dynamical systems, especially when an important dissipation mechanism is involved. When this is the case, the instabilities, bifurcations, limit cycles and attractors are indeed often similar to their finite-dimensional counterparts (see, e.g., [1]). By contrast, when dissipative mechanisms do not exist or are very small in partial differential equations, these may exhibit phenomena that have no counterparts in finite-dimensional systems. Examples of such phenomena include non-dissipative relaxation and asymptotic stability [2]–[4], solitons, as well as the appearance of an infinite number of conserved quantities and an infinite number of steady states [5]–[8].

In this work, we are interested in studying the rare events or large deviations [9] of systems possessing continuous sets of steady states which effectively act as attractors. Such sets of steady states are found in many dynamical equations having a non-canonical Hamiltonian structure, such as the 2D Euler equation, the Vlasov equation, magneto-hydrodynamic equations, and the shallow-water equations, to mention only a few examples; see [5, 8] for more. In all of these examples, the consequence of the non-canonical structure is the existence of an infinite number of conserved quantities or Casimirs, which are responsible for the infinite (and continuous) set of steady states [5, 8]. Physically, these states are important because they can act as attractors, as has been found in experiments [10, 11] and numerical simulations [12]. Moreover, in some cases,

their attractive behavior can be explained theoretically [3, 4] using arguments and methods based on statistical mechanics [8], [13]–[15].

The problem that we address here is how the existence of a continuous set of steady states of a system influences its large deviation properties and how these properties compare with those of finite-dimensional systems. For the latter systems, two generic classes of systems have been considered from the large deviation point of view, namely (i) strongly dissipative systems with well-defined and disconnected attractors, as exemplified by the gradient dynamics of a Brownian particle in a potential (Kramers problem) [16], and (ii) weakly perturbed Hamiltonian systems with added weak friction and noise. The large deviations of both of these classes are well known: they can be obtained using semi-classical (WKB or instanton) approximations of path integrals [9], [17]–[22] or, more rigorously, using the theory developed by Freidlin and Wentzell [23].

Dynamical systems having an infinite number of steady states do not strictly fall in either of these generic classes. The fact that the dynamics of these systems is effectively irreversible and converges towards attractors that are asymptotically stable suggests that they are analogous to the class of strongly dissipative systems. However, because their steady states form one or several connected sets, the presence of a weak noise should lead these systems to diffuse over their attractors, as is the case for Hamiltonian systems. From this point of view, systems with infinite steady states share aspects of both strongly dissipative systems and weakly perturbed Hamiltonian systems.

To illustrate this point, we consider in this paper a simple model with two degrees of freedom, denoted by  $A$  and  $B$ , having a continuous set of steady states in the zero-noise limit. Our goal in the following is to obtain the stationary probability density  $P(A, B)$  of this model, which we refer to simply as the  $AB$  model, in the low-noise limit  $\nu \rightarrow 0$ , where  $\sqrt{\nu}$  is the noise amplitude. Following the theory of large deviations, we expect this density to have the approximate form

$$P(A, B) \approx e^{-c_\nu I(A, B)}, \quad (1)$$

in the limit  $\nu \rightarrow 0$ , where  $c_\nu$  is a coefficient, called the speed, which diverges as  $\nu \rightarrow 0$ , and  $I(A, B)$  is a  $\nu$ -independent function, called the rate function or quasi-potential. Large deviation approximations of this form have been extensively studied, as mentioned above, for various noise-perturbed dynamical systems, including systems with single-point attractors as well as systems with attracting limit cycles (see, e.g., [17]–[22]). In nearly all the classical examples that we are aware of, the speed of the large deviation approximation is  $1/\nu$ . In the case, for example, of a Langevin dynamics describing the overdamped motion of a Brownian particle in a potential  $V(x)$  and in a fluid at temperature  $T$ , the speed is  $1/(k_B T)$ , with  $k_B$  the Boltzmann constant, while the rate function is the potential  $V(x)$ . The resulting large deviation form for the stationary density,

$$P(x) \approx e^{-V(x)/(k_B T)}, \quad (2)$$

is in agreement with the known Arrhenius factor describing the transition probability between stable or metastable states (Kramers theory), and implies, as physically expected, that  $P(x)$  concentrates in the low-noise limit (or low-temperature limit) on the equilibrium state minimizing the potential.

The results that we obtain for the  $AB$  model show that  $P(A, B)$  concentrates in a similar way on the set of stable steady states of the model—in this case, a whole line of

steady states—but does so, in contrast with the classical cases, with a speed proportional to  $1/\sqrt{\nu}$ . Moreover, we show that close to the line of stable steady states, there is a correction to this large deviation approximation having a speed proportional to  $1/\nu$ . For a small but finite noise power  $\nu$ ,  $P(A, B)$  is therefore the sum of two contributions: a large deviation approximation with speed  $1/\sqrt{\nu}$ , which accurately describes the form of  $P(A, B)$  away from the attractor, and a large deviation approximation with speed  $1/\nu$ , which describes  $P(A, B)$  close to the attractor.

These competing large deviation terms are related in the  $AB$  model to different types of fluctuation path having different large deviation speeds and, notably, to fluctuation paths of zero action, which we call ‘sub-instantons’. They are not related, we should mention, to the divergence of the sub-leading prefactors entering in the large deviation approximation, discussed, e.g., by Berglund and Gentz [24, 25]. We argue in the concluding section of this paper that these sub-instantons should arise in more general systems having multiple connected sets of steady states, and that they should lead, as in the  $AB$  model, to stationary probability densities having competing large deviation terms in the low-noise limit.

The rest of the paper is organized as follows. In section 2, we introduce the  $AB$  model, and then proceed in sections 3–5 to obtain  $P(A, B)$  using three different approaches: a path integral approach which leads to results similar to those obtained in the framework of the Freidlin–Wentzell theory (section 3), a dynamical approach based on certain approximations of the  $AB$  model (section 4), and an approach based on the Hamilton–Jacobi equation (section 5). Throughout these sections, the analytical results obtained are compared with numerical results obtained by solving the Fokker–Planck equation directly. We conclude in section 6 with some remarks on the generality of our results.

## 2. Model

The model that we study is defined by the following set of two coupled (Itô) stochastic differential equations (SDEs):

$$\begin{aligned} dA &= (-AB - \nu A) dt + \sigma_A \sqrt{\nu} dW_A \\ dB &= (A^2 - \nu B) dt + \sigma_B \sqrt{\nu} dW_B, \end{aligned} \quad (3)$$

where  $\nu > 0$  is a real coefficient that balances, together with the positive constants  $\sigma_A$  and  $\sigma_B$ , the dissipation of the model and the intensity of the two uncorrelated Brownian motions  $W_A(t)$  and  $W_B(t)$ . Henceforth we refer to this model simply as the  $AB$  model. Note that the inclusion of the two dissipative or friction forces  $-\nu A$  and  $-\nu B$  prevents the system from escaping (by diffusion) to  $B = \infty$  as  $t \rightarrow \infty$ , and makes sure, therefore, that a stationary density  $P(A, B)$  exists.

The zero-noise and zero-friction dynamics of the  $AB$  model is given by

$$\dot{A} = -AB \quad \dot{B} = A^2. \quad (4)$$

This simple dynamics has the key properties that we referred to in the introduction, namely the following.

- (i) It has a continuous set of steady states, which corresponds here to the line  $A = 0$ .

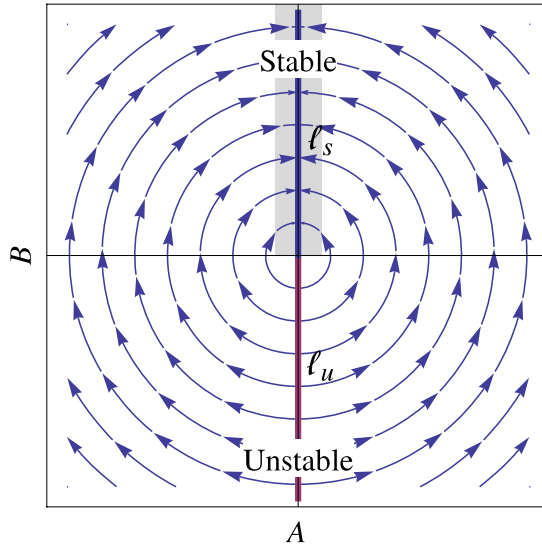


**Figure 1.** The vector field of the  $AB$  model giving rise to a line  $\ell_s$  of stable fixed points and a line  $\ell_u$  of unstable fixed points.

- (ii) The dynamics is irreversible and converges to an attractor, corresponding here to the upper semi-line  $A = 0, B > 0$ , which we denote by  $\ell_s$ . This semi-line is a line of stable steady states or stable fixed points, as shown in figure 1. The lower semi-line  $A = 0, B < 0$ , denoted by  $\ell_u$ , is a line of unstable fixed points<sup>3</sup>.
- (iii) The  $AB$  dynamics conserves the quantity  $E = A^2 + B^2$ , which we refer to as the energy.

These properties are responsible for the competing large deviation scalings of  $P(A, B)$  announced in section 1. We shall show in the next sections that these scalings arise essentially from two very different fluctuation dynamics around  $\ell_s$  and  $\ell_u$ , which will be studied analytically. To support our results, we shall also present numerical results obtained by directly integrating the Fokker–Planck equation associated with equation (3) for different noise powers<sup>4</sup>. Some of these results are shown in figure 2 as contour plots of  $P(A, B)$ . We can already see from this figure that  $P(A, B)$  concentrates on the stable line  $\ell_s$  as  $\nu \rightarrow 0$ , and that it is otherwise relatively isotropic away from  $\ell_s$ . Our analytical study of the  $AB$  model and of its fluctuations around  $\ell_s$  and  $\ell_u$  will explain these two properties, among others. The main result that we shall obtain for  $\sigma_A = \sigma_B = 1$  is the large deviation result

$$\lim_{\nu \rightarrow 0} -\sqrt{\nu} \ln P(x) = I(A, B), \quad (5)$$

<sup>3</sup> The connecting point  $(0, 0)$  is marginally stable.

<sup>4</sup> The numerical integration was carried out with the routine `NDSolve` of Mathematica using double-digit accuracy and standard vanishing boundary conditions for square domains of the  $A$ – $B$  plane. The domains used were  $[-5, 5]^2$  for  $\nu = 0.5$  and  $\nu = 0.1$ ,  $[-4, 4]^2$  for  $\nu = 0.05$ , and  $[-2, 2]^2$  for  $\nu = 0.025$ . Only a portion of these regions is shown in figure 2.

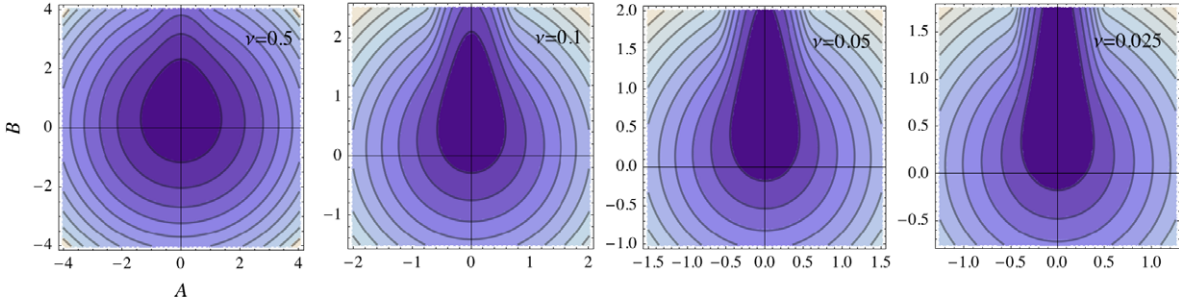


**Figure 2.** Contour plots of  $P(A, B)$  obtained by direct numerical integration of the Fokker–Planck equation associated with the  $AB$  model for  $\sigma_A = \sigma_B = 1$ . The noise intensity  $\nu$  used in the integration is shown in the plots. Darker colors correspond to larger values of  $P(A, B)$ . The region plotted for each noise power is different to highlight the concentration around the stable line.

with

$$I(A, B) = \frac{2\sqrt{2}}{3}(A^2 + B^2)^{3/4}, \tag{6}$$

away from the stable line  $\ell_s$ . We shall also describe corrections of this large deviation result for finite values of  $\nu$  near  $\ell_s$ .

### 3. Path integral solution

We give in this section a first derivation of the large deviation form of  $P(A, B)$  following the classical theory of Freidlin and Wentzell [23]. This calculation is valid near the line  $\ell_s$  of stable points and yields the large deviation speed  $c_\nu = 1/\nu$ .

#### 3.1. Classical theory

Consider a diffusion process  $\{X(t)\}$  in  $\mathbb{R}^D$  which is the solution of the SDE

$$dX(t) = f(X(t)) dt + \sqrt{\nu} dW(t), \tag{7}$$

where  $dW(t)$  are increments of the Brownian motion. It is known from the work of Freidlin and Wentzell (F–W) that the stationary density  $P(x)$  of this process satisfies, under certain conditions, a large deviation form or large deviation principle (LDP) in the low-noise limit  $\nu \rightarrow \infty$ , which we informally write as

$$P(x) \approx e^{-V(x)/\nu}, \tag{8}$$

to mean

$$\lim_{\nu \rightarrow \infty} -\nu \ln P(x) = V(x). \tag{9}$$

Moreover, from the F–W theory, it is known that the rate function or pseudo-potential  $V(x)$  defined by this limit can be obtained from the following minimization problem:

$$V(x) = \inf_{t>0} \inf_{x(0) \in O, x(t)=x} L[x] \tag{10}$$

which involves the Lagrangian or action

$$L[x] = \int_0^t \mathcal{L}(\dot{x}, x) ds, \quad \mathcal{L}(\dot{x}, x) = \frac{1}{2}(\dot{x} - f(x))^2, \quad (11)$$

associated with a path  $\{x(s)\}_{s=0}^t$  of the process. The minimization in (10) is performed over all paths starting on the attractor  $O$  of the system at time  $t = 0$  and reaches the point  $x$  after a time  $t$  which is usually taken to go to infinity.

The LDP for  $P(x)$  is akin to the semi-classical or WKB approximation of quantum mechanics, and can be explained heuristically as in quantum mechanics by expressing  $P(x)$  in path integral form:

$$P(x) = \lim_{t \rightarrow \infty} P(x, t | x \in O, 0) = \lim_{t \rightarrow \infty} \int_{x(0) \in O}^{x(t)=x} \mathcal{D}[x] e^{-L[x]/\nu}, \quad (12)$$

and by arguing that the probability to reach a point  $x$  is given, in the low-noise limit  $\nu \rightarrow 0$ , by the most probable path, called the optimal path or instanton, which starts on the attractor and reaches that point after a very long time. As this optimal path must have a minimal action under the terminal constraint  $x(0) \in O$  and  $x(t) = x$ , we recover the result of (10).

Freidlin and Wentzell [23] showed that this heuristic argument based on path integrals is rigorously valid for the SDE (7) provided essentially that  $O$  is a unique point attractor of the deterministic dynamics  $\dot{x} = f(x)$ . If this dynamics admits many point attractors, then the result of equation (10) holds locally in regions  $G \subset \mathbb{R}^D$  that enclose single attractors and do not include characteristic boundaries, such as separatrices. Graham [17, 26] also showed semi-heuristically that the F–W theory can be applied for non-point attractors, e.g., limit cycles or strange attractors.

Here we apply the F–W theory to the  $AB$  model in a local sense by considering a region of the upper half-plane  $B > 0$  surrounding the attracting line  $\ell_s$  (see the gray region in figure 1). As we take the limit  $\nu \rightarrow 0$ , we neglect the dissipative terms  $-\nu A$  and  $-\nu B$  in the full action of the model. Therefore, the action that we consider in the minimization problem is

$$L[A, B] = \int_0^t \mathcal{L} ds, \quad \mathcal{L} = \frac{1}{2\sigma_A^2}(\dot{A} + AB)^2 + \frac{1}{2\sigma_B^2}(\dot{B} - A^2)^2. \quad (13)$$

The reason for neglecting the dissipative terms in the action is that they are sub-dominant in the low-noise limit compared with the other terms, and lead to correction terms of order  $\nu$  in the rate function  $I(A, B)$ . The net effect of neglecting these terms when solving the minimization problem of (10) is to look for instantons that emanate anywhere from the stable line  $\ell_s$  of fixed points, which is the attractor of noiseless  $AB$  dynamics without the dissipation forces, i.e., equations (4), rather than emanating from the origin  $(0, 0)$ , which is the attractor of the noiseless  $AB$  dynamics with the dissipative forces.

To find the instantons emanating from  $\ell_s$ , we can solve the Euler–Lagrange equations

$$\frac{d}{ds} \frac{\partial \mathcal{L}}{\partial \dot{A}} - \frac{\partial \mathcal{L}}{\partial A} = 0 \quad \frac{d}{ds} \frac{\partial \mathcal{L}}{\partial \dot{B}} - \frac{\partial \mathcal{L}}{\partial B} = 0, \quad (14)$$

where  $\mathcal{L}$  is the Lagrangian density defined in equations (13), with the boundary conditions  $A(0), B(0) \in \ell_s$  and  $A(t) = A, B(t) = B$ . By finding the solution of this equation for an

increasing ‘hitting’ time  $t$ , we then find a succession of approximations of the rate function  $I(A, B)$ , which converge to  $I(A, B)$  as  $t \rightarrow \infty$ .

For the  $AB$  model, the Euler–Lagrange equations read explicitly

$$\begin{aligned} \frac{1}{\sigma_A^2}(\ddot{A} + A\dot{B} - AB^2) - \frac{2}{\sigma_B^2}(A^3 - A\dot{B}) &= 0 \\ \frac{1}{\sigma_A^2}(A^2B + A\dot{A}) - \frac{1}{\sigma_B^2}(\ddot{B} - 2A\dot{A}) &= 0. \end{aligned} \quad (15)$$

This is a set of nonlinear, second-order equations of motion, which can be solved only numerically. In practice, it is easier to solve these equations by transposing them into an equivalent set of first-order Hamiltonian equations of motion defined by

$$\dot{A} = \frac{\partial \mathcal{H}}{\partial \rho_A}, \quad \dot{B} = \frac{\partial \mathcal{H}}{\partial \rho_B}, \quad \dot{\rho}_A = -\frac{\partial \mathcal{H}}{\partial A}, \quad \dot{\rho}_B = -\frac{\partial \mathcal{H}}{\partial B}, \quad (16)$$

where

$$\rho_A = \frac{\partial \mathcal{L}}{\partial \dot{A}}, \quad \rho_B = \frac{\partial \mathcal{L}}{\partial \dot{B}} \quad (17)$$

are the conjugate momenta associated with  $A$  and  $B$ , respectively, and

$$\mathcal{H} = \rho_A \dot{A} + \rho_B \dot{B} - \mathcal{L} \quad (18)$$

is the Hamiltonian density. For the  $AB$  model, the Hamiltonian equations are explicitly

$$\begin{aligned} \dot{A} &= \sigma_A^2 \rho_A - AB, & \dot{B} &= \sigma_B^2 \rho_B + A^2, \\ \dot{\rho}_A &= \rho_A B - 2\rho_B A, & \dot{\rho}_B &= \rho_A A. \end{aligned} \quad (19)$$

To numerically solve these equations, we use the fact that  $\mathcal{H}$  is conserved in time and that  $\mathcal{H} = 0$  on the attractor  $\ell_s$ . As a result, the instantons are such that  $\mathcal{H} = 0$  for all times. Moreover, since the dynamics from the attractor is unstable, we numerically integrate the Hamiltonian equations backward in time instead of forward in time. This means that we start the integration from the point  $(A, B)$ , and find initial conditions for  $\rho_A$  and  $\rho_B$  such that the time-reverse dynamics of (19) leads to the attractor  $\ell_s$ .

A number of instantons obtained from this procedure are shown in figure 3 for different points  $(A, B)$  in the first quadrant of the  $A$ – $B$  plane<sup>5</sup>. The action associated with these paths, which yields the rate function  $I(A, B)$  according to equation (10), is shown in figure 4 as data points. The speed associated with this rate function is  $1/\nu$ . In the same figure, we show with the full and dashed lines the results of analytical calculations presented in section 5. The agreement between the two sets of results will be discussed in more detail in these sections.

An interesting property of the instantons, seen from figure 3, is that they are different from the natural decay paths of the system, i.e., the paths of the deterministic dynamics starting from a point  $(A, B)$  away from the attractor and ending on the attractor (shown in blue). This difference is characteristic of SDEs that are not gradient, i.e., which cannot

<sup>5</sup> By the symmetry of the  $AB$  model, the instantons of the second quadrant, i.e., on the left of  $\ell_s$ , must be the mirror images of the instantons of the first quadrant.

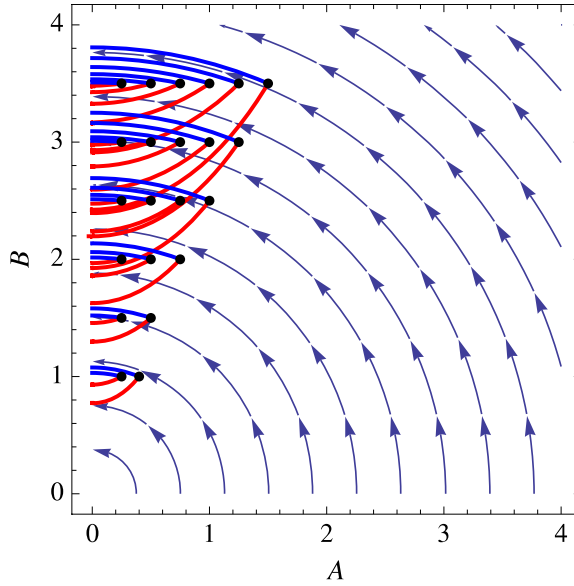


**Figure 3.** Red lines: instantons reaching certain points  $(A, B)$  (black dots) from the stable attracting line of the  $AB$  model. Blue lines: deterministic paths connecting the same points back to the stable attractor according to the noiseless dynamics of the  $AB$  model. Parameters:  $\sigma_A = \sigma_B = 1$ .

be written in the form

$$\dot{x} = -\nabla U(x) + \sqrt{\nu} \xi(t) \quad (20)$$

for a scalar function  $U(x)$ . It is known that if such a form exists, then the rate function  $I(x)$  associated with the stationary distribution  $P(x)$  is simply given by  $I(x) = 2U(x)$ . In this case, we moreover have that the instantons are the time-reversed version of the natural decay paths.

For the  $AB$  model, these results do not apply: the SDE (3) is not of gradient-type, which means that we must explicitly solve the Euler–Lagrange equations or the equivalent Hamiltonian equations to find the instantons and their associated action. Physically, this also means that the  $AB$  model is a nonequilibrium system that violates detailed balance and gives rise to a non-vanishing probability current  $J = (J_A, J_B)^T$ , whose components are here given by

$$\begin{aligned} J_A &= (-AB - \nu A)P(A, B) - \frac{\nu\sigma_A^2}{2} \frac{\partial P(A, B)}{\partial A}, \\ J_B &= (A^2 - \nu B)P(A, B) - \frac{\nu\sigma_B^2}{2} \frac{\partial P(A, B)}{\partial B}. \end{aligned} \quad (21)$$

This current is actually a current loop, as shown in figure 5: it has the shape of a ‘squashed’ double-solenoid and circulates through the origin.

### 3.2. Sub-instantons

The instantons shown in figure 3 are not strictly speaking the only possible instantons that the  $AB$  model admits. Interestingly, it is also possible to reach any points  $(A, B)$

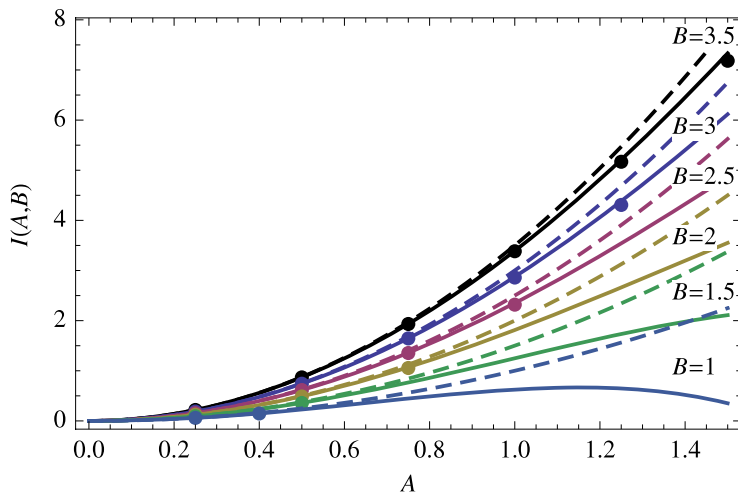


**Figure 4.** The rate function  $I(A, B)$  near  $\ell_s$  as a function of  $A$  for different values of  $B$ . Data points: rate function obtained from the instantons shown in figure 3. Dashed and full lines: second- and fourth-order approximations, respectively, of  $I(A, B)$  obtained from the Hamilton–Jacobi method; see section 5. Parameters:  $\sigma_A = \sigma_B = 1$ .

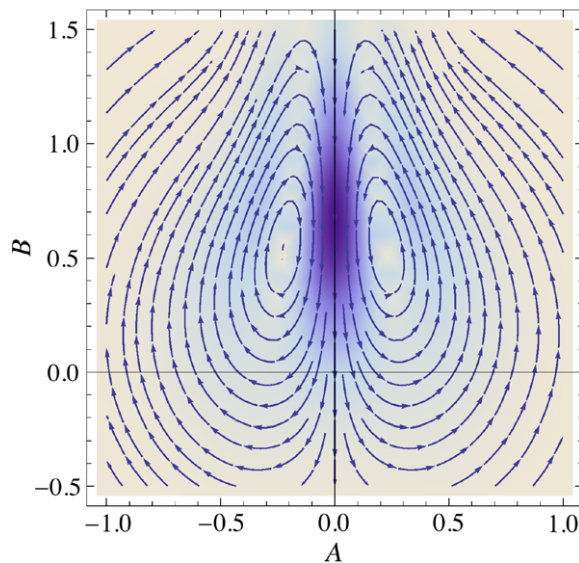


**Figure 5.** Streamlines of the probability current  $J$  for  $\nu = 0.05$  and  $\sigma_A = \sigma_B = 1$ , with level colors representing  $|J|$ . The darker colors correspond to larger current magnitudes.

from the attractor by following a fluctuation path constructed as follows (see figure 6).

- (i) Start from any point on the stable attractor and go down to the origin.
- (ii) Follow the line  $\ell_u$  of unstable fixed points down to the point  $(0, B')$  such that  $B'^2 = A^2 + B^2$ .
- (iii) Follow the natural orbit of energy  $E = A^2 + B^2$  connecting  $(0, B')$  to  $(A, B)$ .

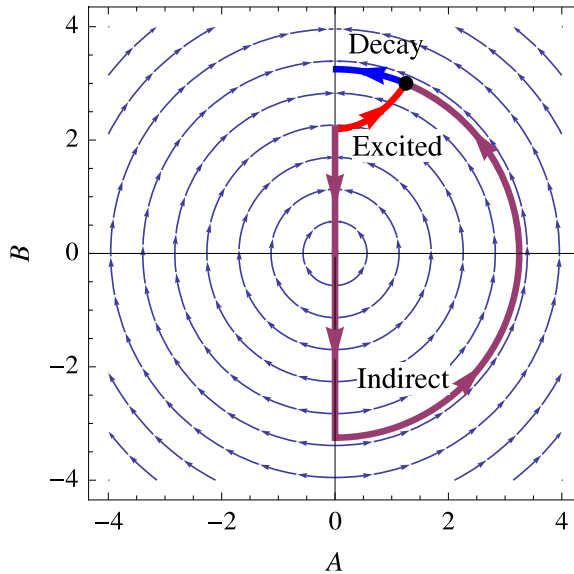


**Figure 6.** Optimal paths. The point in black in the  $A$ - $B$  plane can be reached either by a direct, excited path (in red) with positive action or by an indirect path (in purple) that first goes along the stable and unstable lines of fixed points, and then follows a natural trajectory of the deterministic dynamics. The latter path has a null action.

As each of these parts either lies on the line of stable and unstable points or follows a natural path of the deterministic system, the complete path thus constructed must have a zero action on the large deviation scale  $1/\nu$ .

The existence of these zero-action instantons, or sub-instantons as we shall call them, gives us an indication that the dominant behavior of  $P(A, B)$  does not have a speed  $1/\nu$ ; in fact it has a speed  $1/\sqrt{\nu}$ , as we shall see below. The crucial point to note, however, is that  $P(A, B)$  has a sub-dominant LDP with speed  $1/\nu$  near the attractor  $\ell_s$  (see the gray region in figure 1), which is precisely the LDP that we have obtained before with the F-W calculation. This sub-dominant LDP arises from instantons having a non-zero action emanating from  $\ell_s$ , whereas the dominant LDP, which scales with  $1/\sqrt{\nu}$ , is related to fluctuation paths that are sub-instantons. The fact that these sub-instantons follow in the end the deterministic dynamics explains the observed isotropy of  $P(A, B)$  away from  $\ell_s$ , i.e., why  $P(A, B)$  has constant level curves along the vector field of the  $AB$  noiseless dynamics. The same indirect fluctuation paths also explain the existence of the probability current mentioned before.

We show in the next two sections how to go beyond the F-W calculation to obtain the dominant LDP of  $P(A, B)$ . Two methods are presented: the first is based on the solution of a timescale separation of the solution of the  $AB$  model, whereas the second is based on a direct approximation of the solution of the Fokker-Planck equation.

#### 4. Dynamical analysis

We analytically derive in this section LDPs for  $P(A, B)$  near  $\ell_s$  and then near  $\ell_u$  using the insight gained in section 3. In treating  $\ell_s$  and  $\ell_u$  separately, we shall see how the stable

and unstable dynamics, respectively, of each of these lines give rise to different LDPs. As a prelude to these calculations, we obtain the stationary probability density of the energy defined by  $E = A^2 + B^2$  to show that it does not scale with  $\nu$ , as is the case for weakly perturbed Hamiltonian systems.

#### 4.1. Energy

Given the original system of equations for  $A$  and  $B$ , displayed in equation (3),  $E$  is found to evolve according to the Itô SDE:

$$dE = -2\nu E dt + \nu (\sigma_A^2 + \sigma_B^2) dt + 2\sqrt{\nu} (\sigma_A A dW_A + \sigma_B B dW_B). \quad (22)$$

This equation is not closed—it explicitly depends on  $A$  and  $B$ —but the equation for the mean energy is closed:

$$\frac{1}{\nu} \frac{d \langle E \rangle}{dt} = -2 \langle E \rangle + (\sigma_A^2 + \sigma_B^2). \quad (23)$$

From this, we find the stationary mean energy

$$\langle E \rangle_s = \frac{\sigma_A^2 + \sigma_B^2}{2}. \quad (24)$$

To find  $P(E)$ , we solve the Fokker–Planck equation associated with the Langevin equation for  $E$ . For simplicity, consider first the case  $\sigma_A = \sigma_B = \sigma$  and let  $\phi$  be any test function. Applying Itô’s formula and averaging over the noises, we obtain

$$\frac{1}{2\nu} \frac{d \langle \phi(E) \rangle}{dt} = \langle (\sigma^2 - E) \phi'(E) \rangle + \sigma^2 \langle E \phi''(E) \rangle. \quad (25)$$

The associated Fokker–Planck equation for the energy pdf  $P(E, t)$  is thus

$$\frac{1}{2\nu} \frac{\partial P}{\partial t} = \frac{\partial}{\partial E} \left[ (E - \sigma^2) P + \sigma^2 \frac{\partial}{\partial E} (EP) \right], \quad (26)$$

and admits the following stationary solution  $P(E)$ :

$$P(E) = \frac{1}{\sigma^2} e^{-E/\sigma^2}. \quad (27)$$

It is easy to verify from this result that  $\langle E \rangle_s = \sigma^2$ , in accordance with the exact result of equation (24). Note also that  $P(E)$  does not depend on  $\nu$ , as announced, which means that there is no LDP for  $P(E)$ .

For the case  $\sigma_A \neq \sigma_B$ , Itô’s formula leads to

$$\frac{1}{2\nu} \frac{d \langle \phi(E) \rangle}{dt} = \left\langle \left( \frac{\sigma_A^2 + \sigma_B^2}{2} - E \right) \phi'(E) \right\rangle + \langle (\sigma_A^2 A^2 + \sigma_B^2 B^2) \phi''(E) \rangle, \quad (28)$$

which is exact for any test function  $\phi$ . By contrast with equation (25), the equation above is not a closed equation for  $E$  as the variables  $A$  and  $B$  are involved. However, because the typical values of the variable  $A$  are of order  $\sqrt{\nu}\sigma_1/\sqrt{B}$ , which is much smaller than both  $\sqrt{E}$  and  $B$  as soon as  $E \gg \nu^2\sigma_1^4$ , it is natural in equation (28) to make the approximations  $B^2 \simeq E$  and  $A^2 \ll E$ . One then obtains a closed equation for  $\phi(E)$  whose associated

Fokker–Planck equation is

$$\frac{1}{2\nu} \frac{\partial P}{\partial t} = \frac{\partial}{\partial E} \left[ \left( E - \frac{\sigma_A^2 + \sigma_B^2}{2} \right) P + \sigma_B^2 \frac{\partial}{\partial E} (EP) \right]. \quad (29)$$

The stationary solution of this equation is

$$P(E) = C E^{(\sigma_A^2 - \sigma_B^2)/(2\sigma_B^2)} e^{-E/\sigma_B^2}, \quad (30)$$

where  $C$  is a normalization constant. We can verify that this expression reduces to the one we found in equation (27) when  $\sigma_A = \sigma_B = \sigma$ . It is also easily verified that the average energy obtained from this distribution is given by the exact relation displayed in equation (24).

## 4.2. Dynamics around stable fixed points

We now derive a local LDP for  $P(A, B)$  around  $\ell_s$  (see the gray region in figure 1) using the fact that there exists a separation between the time with which  $A$  relaxes to 0 (time of order  $1/B$ ) and the time with which  $E$  varies (time of order  $1/\nu$ ). Since  $E \approx B^2$  for  $A$  close to 0, the slow dynamics of  $E$  translates into a slow dynamics of  $B$ , which can be treated adiabatically with respect to  $A$ . Thus, we consider  $B$  to be constant and study the dynamics of the rapid variable  $A$  given by the first equation of the  $AB$  model:

$$dA = (-AB - \nu A) dt + \sigma_A \sqrt{\nu} dW_A. \quad (31)$$

For fixed  $B$ , this equation is linear in  $A$ , which means that  $A$  evolves according to an Ornstein–Uhlenbeck process. In the stationary state,  $A$  is of order  $\sqrt{\nu}$  and the term  $\nu A$  can be considered negligible, and so we find

$$P(A|B) = \sqrt{\frac{B}{\pi\nu\sigma_A^2}} \exp\left(-\frac{BA^2}{\nu\sigma_A^2}\right) \quad (32)$$

for the stationary distribution of the fast variable  $A$  given that  $B$  is fixed. This stationary distribution is reached on a timescale of order  $1/B$ .

Next, we study the evolution of  $B$  given by

$$dB = \nu(A'^2 - B) dt + \sqrt{\nu} \sigma_B dW_B, \quad (33)$$

using  $A' = A/\sqrt{\nu}$ . As we did for  $A$ , we can approximate  $A'$  to be an Ornstein–Uhlenbeck process with variance  $\langle A'^2 \rangle = \sigma_A^2/(2B)$ . Accordingly, the fluctuations of the variable  $\nu A'^2$  must be such that  $\langle (\nu A'^2 - \langle \nu A'^2 \rangle)^2 \rangle$  is of order  $\nu^2$ . Such fluctuations are much smaller than the effect of the white noise for  $B$ , and so, to leading order in  $\nu$ , the fluctuations of  $A'^2$  can be neglected. The approximate dynamics for  $B$  to leading order in  $\nu$  is thus

$$dB = \nu \left( \frac{\sigma_A^2}{2B} - B \right) dt + \sqrt{\nu} \sigma_B dW_B. \quad (34)$$

The associated Fokker–Planck equation is

$$\frac{1}{\nu} \frac{\partial P}{\partial t} = \frac{\partial}{\partial B} \left[ \left( B - \frac{\sigma_A^2}{2B} \right) P + \frac{\sigma_B^2}{2} \frac{\partial P}{\partial B} \right], \quad (35)$$

and has for stationary solution

$$P(B) = C B^{\sigma_A^2/\sigma_B^2} e^{-B^2/\sigma_B^2}, \quad (36)$$

where  $C$  is a normalization constant. By combining this solution with the solution found for  $P(A|B)$ , we thus find

$$P(A, B) = P(A|B)P(B) = C B^{(2\sigma_A^2+1)/2\sigma_B^2} \exp\left(-\frac{B^2}{\sigma_B^2} - \frac{BA^2}{\nu\sigma_A^2}\right), \quad (37)$$

where  $C$  is again a normalization constant. The LDP extracted from this result has the form

$$P(A, B) \approx e^{-I(A,B)/\nu}, \quad I(A, B) = -\frac{BA^2}{\sigma_A^2}, \quad (38)$$

and is nothing but the LDP associated with  $P(A|B)$ . This shows that the large deviations of the  $AB$  model around the attractor are mainly the result of the diffusive fluctuations of  $A$  for  $B$  constant.

The rate function  $I(A, B)$  of equation (38) is shown in figure 4 as a function of  $A$  and for different values of  $B$  as dashed lines. We see that there is a favorable comparison between this rate function and the rate function obtained from the F–W theory (represented again by the data points). The difference from the F–W results can be explained by noting that the rate function derived in this section is only a second-order approximation of the rate function obtained by approximating the instantons as straight, horizontal paths joining a point  $(0, B)$  on  $\ell_s$  to a point  $(A, B)$  near  $\ell_s$ . The correct instantons, as seen from figure 3, have a certain inclination or curvature in the  $B$  direction, which has the effect of reducing slightly the action of straight, constant- $B$  paths. We shall see in section 5 that the Hamiltonian–Jacobi method is able to capture this effect as a fourth-order correction to  $I(A, B)$ .

### 4.3. Dynamics around unstable fixed points

To obtain  $P(A, B)$  around the line  $\ell_u$  of unstable fixed points, we need to construct a different approximation of the  $AB$  dynamics that accounts for the fact that trajectories starting at the origin have a small probability of diffusing down the line  $\ell_u$  and that, as soon as they depart from this line, they are rapidly expelled along the force lines of the  $AB$  dynamics, to reach the stable line  $\ell_s$ ; see figures 1 and 6. This dynamics creates a probability current because, eventually, the trajectories return to the origin by diffusing down the line  $\ell_s$  and start new loops by diffusing again down  $\ell_u$ .

In order to qualitatively understand this fluctuation dynamics, we consider the following approximation of the  $AB$  model:

$$\begin{aligned} dA &= \alpha_A A dt + \sigma_A \sqrt{\nu} dW_A, \\ dB &= -\nu B dt + \sigma_B \sqrt{\nu} dW_B, \end{aligned} \quad (39)$$

which involves a ‘top-hill’ diffusion process for  $A$  ( $\alpha_A > 0$ ) and a ‘down-hill’ diffusion for  $B$ . The equation for  $B$  is the exact dynamics of  $B$  on the line  $A = 0$ , whereas the ‘top-hill’ term  $\alpha_A A$  is analogous to the term  $-AB$  in the original  $AB$  model. For now, we consider  $\alpha_A$  to be independent of  $B$  in order to have a solvable model which will help us to gain

a qualitative understanding of the unstable dynamics. We discuss the case  $\alpha_A = -B$  at the end of this section.

For  $\alpha_A$  constant, equation (39) describes an unstable linear Gaussian process. To find a stationary distribution  $P(A, B)$  for this process, we have to consider that there is a probability (or current) source at the origin  $O$ . In this case, the probability to reach a point  $(A, B)$  in the lower plane is given by integrating the probability  $P(A, B, t|O)$  that a trajectory starting at the origin  $O$  reaches the point  $(A, B)$  after a variable time  $t$ , to which we multiply the stationary probability density of starting at  $O$ :

$$P(A, B) = P(O) \int_0^\infty P(A, B, t|O) dt. \quad (40)$$

For the decoupled dynamics of equation (39), the propagator  $P(A, B, t|O)$  is simply given by

$$P(A, B, t|O) = \frac{1}{2\pi\sqrt{\langle A^2 \rangle \langle B^2 \rangle}} \exp \left[ - \left( \frac{A^2}{2\langle A^2 \rangle} + \frac{B^2}{2\langle B^2 \rangle} \right) \right], \quad (41)$$

where

$$\langle A^2 \rangle = \frac{\sigma_A^2 \nu}{2\alpha_A} (e^{2\alpha_A t} - 1) \quad (42)$$

and

$$\langle B^2 \rangle = \frac{\sigma_B^2}{2} (1 - e^{-2\nu\sigma_B^2 t}). \quad (43)$$

The difference between the behaviors of the variances of  $A$  and  $B$  plays an important role in determining the LDP of  $P(A, B)$  in the low-noise limit. The variance of  $A$  grows exponentially for large times, as a result of the instability of  $\ell_u$ , whereas that of  $B$  goes to a constant on a long timescale of order  $t \sim (2\sigma_B^2\nu)^{-1}$ . Taking the limit  $\nu \rightarrow 0$ , and anticipating that the integral will be dominated by contributions with times such that  $\nu t \ll 1$ , we obtain

$$P(A=0, B) \approx C \int_0^\infty e^{-\alpha_A t - B^2/(2\sigma_B^2\nu t)} dt \quad (44)$$

for the probability density on  $\ell_u$ , with  $C$  a normalization constant. This can be put in the form of a Laplace integral with the change of variables  $t' = \sqrt{\sigma_B^2\nu} t$ :

$$P(A=0, B) \approx C \int_0^\infty e^{-g(t')/\sqrt{\nu}} dt', \quad (45)$$

where

$$g(t') = \frac{\alpha_A}{\sigma_B} t' + \frac{B^2}{2\sigma_B t'}. \quad (46)$$

In the limit  $\nu \rightarrow 0$ , the integral is therefore dominated by its maximum integrand, which is here located at  $t' = B/\sqrt{2\alpha_A}$ . As a result, we find

$$P(A=0, B) \approx e^{-\varphi(B)/\sqrt{\nu}}, \quad \varphi(B) = \frac{\sqrt{2\alpha_A}}{\sigma_B} B. \quad (47)$$

Note the change of speed in this LDP:  $1/\sqrt{\nu}$  instead of  $1/\nu$ .

From this simple ‘top-hill’ linear model, we conclude that the low probability  $P(0, B)$  for the system to be on the unstable line  $\ell_u$  results from the balance between the probability to reach a finite value  $B$  after a time  $t$  and the probability that the system is not expelled by the unstable dynamics before this time  $t$ . The rare coincidence of these two conditions gives the large deviation result. The preceding computation suggests that the leading contribution corresponding to these rare events corresponds to an optimal time  $t(B)$  proportional to  $\sqrt{\nu}$ .

This qualitative behavior also correctly describes the exact  $AB$  dynamics with  $\alpha_A = B$ . In this case, one can explicitly solve the two equations shown in (39) with  $\alpha_A = B$ . However, we have found it more convenient to use in this case an asymptotic expansion of the Hamilton–Jacobi equation, which we discuss in the next section. For now, we just note that substituting  $\alpha_A = B$  in equation (47) leads to  $\varphi(B) \propto B^{3/2}/\sigma_B$ , a result that will be confirmed in section 5.

To close this section, note that the density  $P(A, B)$  away from  $\ell_u$  is obtained by radially radiating the value of  $P(0, B)$  obtained above, i.e., by setting  $P(A', B') = P(0, B)$  for all  $(A', B')$  such that  $A'^2 + B'^2 = B^2$ . This is expected from the numerical results shown in figure 2 and follows, more precisely, by noticing that trajectories departing infinitesimally from  $\ell_u$  are radiated radially by the vector field of the  $AB$  model. As this instability results only from the deterministic part of the  $AB$  equations, the probability density must have circular level curves.

## 5. Hamilton–Jacobi approach

We give in this section a different derivation of the LDP of  $P(A, B)$  near  $\ell_s$  and  $\ell_u$ , obtained by solving the stationary Fokker–Planck equation of the  $AB$  model, which reads

$$\frac{\partial}{\partial A}(ABP) - \frac{\partial}{\partial B}(A^2P) + \nu \frac{\partial}{\partial A}(AP) + \nu \frac{\partial}{\partial B}(BP) + \nu \frac{\sigma_A^2}{2} \frac{\partial^2 P}{\partial A^2} + \nu \frac{\sigma_B^2}{2} \frac{\partial^2 P}{\partial B^2} = 0. \quad (48)$$

As before, we look for solutions having the LDP form

$$P(A, B) = \phi(A, B) e^{-c_\nu I(A, B)}, \quad (49)$$

where  $I(A, B)$  is the rate function and  $\phi(A, B)$  is a function of  $A$  and  $B$  that does not depend on  $\nu$ . Moreover, following section 4, we choose the noise scaling  $c_\nu = 1/\nu$  around  $\ell_s$  and  $c_\nu = 1/\sqrt{\nu}$  around  $\ell_u$ .

The advantage of the Fokker–Planck method is that it yields more precise expressions for the rate function in the form of series expansions, which are not based, as in the previous section, on approximations of the  $AB$  model. However, to be able to use this method, we need to know the correct large deviation speed of  $P(A, B)$ , i.e., the correct scaling of  $c_\nu$  with  $\nu$ .

### 5.1. Stable fixed points

Inserting the ansatz (49) with  $c_\nu = 1/\nu$  in the Fokker–Planck equation (48) yields, to order  $1/\nu$ , the following partial differential equation:

$$-AB \frac{\partial I}{\partial A} + A^2 \frac{\partial I}{\partial B} + \frac{\sigma_A^2}{2} \left( \frac{\partial I}{\partial A} \right)^2 + \frac{\sigma_B^2}{2} \left( \frac{\partial I}{\partial B} \right)^2 = 0. \quad (50)$$

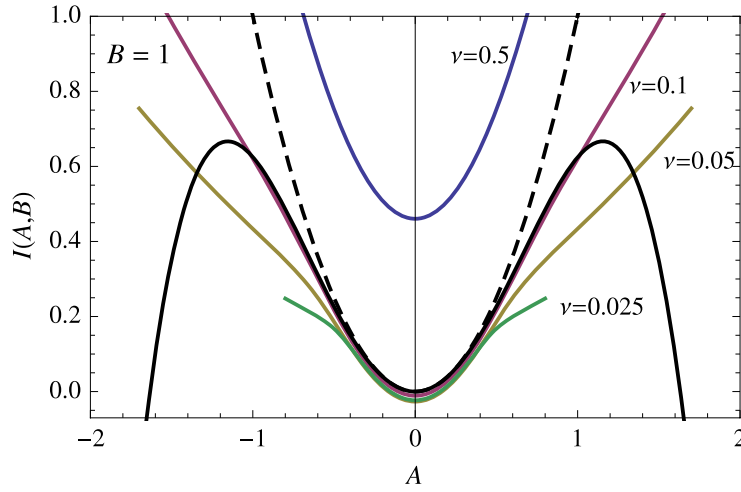


**Figure 7.** Numerical test for  $I(A, B)$ . Black dashed line: second-order result for  $I(A, B)$  obtained from the Hamilton–Jacobi method. Black full line: fourth-order analytical result for  $I(A, B)$  obtained with the same method. Colored lines: rate functions obtained from the numerical integration of the Fokker–Planck equation of the  $AB$  model for different values of  $\nu$ . Parameters:  $\sigma_A = \sigma_B = 1$ .

This is a Hamilton–Jacobi equation corresponding to the weak-noise limit of our model. Unfortunately, we are unable to solve this equation explicitly. However, we expect the solution to be localized close to  $A = 0$ , and so it is natural to look for an expansion of  $I$  for small  $A$ . By the symmetry of the  $AB$  model, the dependence of  $P(A, B)$  on  $A$  must be even. Thus, assuming an expansion of  $I$  of the form

$$I(A, B) = I_0(B) + I_1(B)A^2 + I_2(B)A^4 + O(A^6) \quad (51)$$

in equation (50), we directly obtain

$$I(A, B) = \frac{B}{\sigma_A^2}A^2 - \frac{2\sigma_A^2 + \sigma_B^2}{8\sigma_A^4 B}A^4 + O(A^6). \quad (52)$$

Figure 4 shows how this result compares with the calculation of the rate function based on the instanton approximation presented in section 3. The full colored lines on this plot show  $I(A, B)$ , as given in equation (52), as a function of  $A$  for different values of  $B$ . The dashed colored lines represent the same result but truncated to second order. The data points, as mentioned in section 3, are the results of the instanton approximation. The near perfect match between the data points and the full lines confirm the consistency of the Hamilton–Jacobi and instanton results.

The result of equation (52) is also compared in figure 7 with results obtained by numerically integrating the Fokker–Planck equation. We see in this figure that, for small values of  $\nu$ , the numerical results are relatively close to  $I$ , at least for points  $(A, B)$  near  $\ell_s$ . It must be said that it is rather difficult to obtain reliable results by numerically integrating the Fokker–Planck with small noise intensities, especially away from the attractor. In our case, we could not obtain reliable results for values of  $\nu$  smaller than about  $\nu = 0.025$ . For this reason, the numerical results of figure 7 are presented to check that our analytical

results have the correct scaling in  $\nu$ , and that the rate functions obtained numerically and analytically are qualitatively similar.

To obtain the correction factor  $\phi$ , we need to consider the Hamilton–Jacobi equation for  $\phi$  obtained at order 0 of the Fokker–Planck equation:

$$B\phi + AB\frac{\partial\phi}{\partial A} - A^2\frac{\partial\phi}{\partial B} - A\frac{\partial I}{\partial A}\phi - B\frac{\partial I}{\partial B}\phi - \frac{\sigma_A^2}{2}\left(\frac{\partial^2 I}{\partial A^2}\phi + 2\frac{\partial I}{\partial A}\frac{\partial\phi}{\partial A}\right) - \frac{\sigma_B^2}{2}\left(\frac{\partial^2 I}{\partial B^2}\phi + 2\frac{\partial I}{\partial B}\frac{\partial\phi}{\partial B}\right) = 0. \quad (53)$$

As before, we attempt to solve this equation by expanding  $\phi$  in even powers of  $A$ . Thus we assume

$$\phi(A, B) = \phi_0(B) + \phi_1(B)A^2 + O(A^4), \quad (54)$$

and find at order  $A^2$

$$4(\sigma_A^2 + \sigma_B^2)B\phi'_0 + (12B^2 - 6\sigma_A^2 - 3\sigma_B^2)\phi_0 + 8B^2\sigma_A^2\phi_1 = 0, \quad (55)$$

where  $\phi'_0(B)$  is the  $B$ -derivative of  $\phi_0(B)$ . This equation is not a closed differential equation for  $\phi_0$  as it involves  $\phi_1$ . To get a closed set of equations, we find a complementary equation by looking at the Hamilton–Jacobi equation obtained at order  $\nu$ , which reads

$$B\varphi + AB\frac{\partial\varphi}{\partial A} - A^2\frac{\partial\varphi}{\partial B} + 2\phi - A\frac{\partial I}{\partial A}\varphi + A\frac{\partial\phi}{\partial A} - B\frac{\partial I}{\partial B}\varphi + B\frac{\partial\phi}{\partial B} - \frac{\sigma_A^2}{2}\left(\frac{\partial^2 I}{\partial A^2}\varphi + 2\frac{\partial I}{\partial A}\frac{\partial\varphi}{\partial A} - \frac{\partial^2\phi}{\partial A^2}\right) - \frac{\sigma_B^2}{2}\left(\frac{\partial^2 I}{\partial B^2}\varphi + 2\frac{\partial I}{\partial B}\frac{\partial\varphi}{\partial B} - \frac{\partial^2\phi}{\partial B^2}\right) = 0. \quad (56)$$

We seek a solution of the form  $\varphi(A, B) = \varphi_0(B) + O(A^2)$  for the function  $\varphi$  carrying the  $\nu$ -order correction. Substituting in the equation above the expressions of  $I$  and  $\phi$  shown in (52) and (54), respectively, we obtain at order  $A^0$

$$\sigma_B^2\phi''_0 + 2B\phi'_0 + 4\phi_0 + 2\sigma_A^2\phi_1 = 0. \quad (57)$$

With this equation and equation (55), it is possible to eliminate the function  $\phi_1$  to obtain a closed differential equation for  $\phi_0$ :

$$4B^2\sigma_B^2\phi''_0 + [8B^3 - 4B(\sigma_A^2 + \sigma_B^2)]\phi'_0 + (4B^2 - 6\sigma_A^2 - 3\sigma_B^2)\phi_0 = 0. \quad (58)$$

Looking for solutions of the form  $CB^\alpha e^{-\beta B^2}$ , we then find

$$\phi_0(B) = CB^{(2\sigma_A^2+1)/2\sigma_B^2} e^{-B^2/\sigma_B^2}, \quad (59)$$

where  $C$  is a normalization constant. This is the only normalizable solution to equation (58).

With the solution of  $I$  truncated to order  $O(A^2)$  and  $\phi$  truncated to order  $O(A^0)$ , i.e.,  $\phi = \phi_0 + O(A^2)$ , we can finally write down our approximation for  $P(A, B)$ :

$$P(A, B) \approx \left[ B^{(2\sigma_A^2+1)/2\sigma_B^2} \exp\left(-\frac{B^2}{\sigma_B^2}\right) + O(A^2) \right] \times \exp\left(-\frac{BA^2}{\nu\sigma_A^2} + \frac{2\sigma_A^2 + \sigma_B^2}{8\sigma_A^4 B} A^4 + O(A^6/\nu)\right), \quad (60)$$

which reproduces the result of equation (37) to second order in  $A$  in the exponential.

### 5.2. Unstable fixed points

Knowing from the previous sections that  $P(A, B)$  is isotropic around the line  $\ell_u$  of unstable points, it makes sense to solve the Fokker–Planck equation in polar coordinates:

$$\begin{aligned} \frac{\partial P}{\partial t} = & -\frac{\partial}{\partial r} \left[ \left( -\nu r + \frac{\nu}{2r} (\sigma_A^2 \sin^2 \theta + \sigma_B^2 \cos^2 \theta) \right) P \right] \\ & - \frac{\partial}{\partial \theta} \left[ \left( r \cos \theta - \nu \sin 2\theta + \frac{\nu \sin 2\theta}{2r^2} (\sigma_A^2 + \sigma_B^2) \right) P \right] \\ & + \frac{\nu}{2} \frac{\partial^2}{\partial r^2} \left[ (\sigma_A^2 \cos^2 \theta + \sigma_B^2 \sin^2 \theta) P \right] \\ & + \frac{\nu}{2} \frac{\partial^2}{\partial r \partial \theta} \left[ \left( -\sigma_A^2 \frac{\sin 2\theta}{r} + \sigma_B^2 \frac{\sin 2\theta}{r} \right) P \right] \\ & + \frac{\nu}{2} \frac{\partial^2}{\partial \theta^2} \left[ \left( \sigma_A^2 \frac{\sin^2 \theta}{r^2} + \sigma_B^2 \frac{\cos^2 \theta}{r^2} \right) P \right], \end{aligned} \quad (61)$$

using the large deviation ansatz  $P(A, B) = \phi e^{-I/\sqrt{\nu}}$ . At order  $\nu^{-1/2}$ , and setting  $\sigma_A = \sigma_B = 1$  for simplicity, this equation reduces to the simple partial differential equation

$$-r \cos \theta \frac{\partial I}{\partial \theta} = 0, \quad (62)$$

which shows that  $I$  does not depend on  $\theta$  for  $A \neq 0$  (i.e.,  $\theta \neq \pm\pi/2$ ). To find the  $r$ -dependence of  $I$ , we have to consider the Hamilton–Jacobi equation associated with the zeroth order of the Fokker–Planck equation in  $\nu$ , which reads

$$-\frac{\partial}{\partial \theta} (r \phi \cos \theta) + \frac{1}{2} \left( \frac{dI}{dr} \right)^2 \phi = 0. \quad (63)$$

We look for a solution of this equation close to  $\theta = -\pi/2$  by making the change of variables  $\theta = -\pi/2 + u$  and by defining  $\tilde{\phi}(u, r) = \phi(-\pi/2 + u, r)$ . The equation above then becomes

$$\frac{\partial}{\partial u} (r \tilde{\phi} \sin u) - \frac{1}{2} \left( \frac{dI}{dr} \right)^2 \tilde{\phi} = 0. \quad (64)$$

By symmetry,  $\tilde{\phi}$  must be even in  $u$ , which implies that  $\partial\tilde{\phi}/\partial u = 0$  at  $u = 0$ , and so we find

$$\left[ r - \frac{1}{2} \left( \frac{dI}{dr} \right)^2 \right] \tilde{\phi}(0, r) = 0. \quad (65)$$

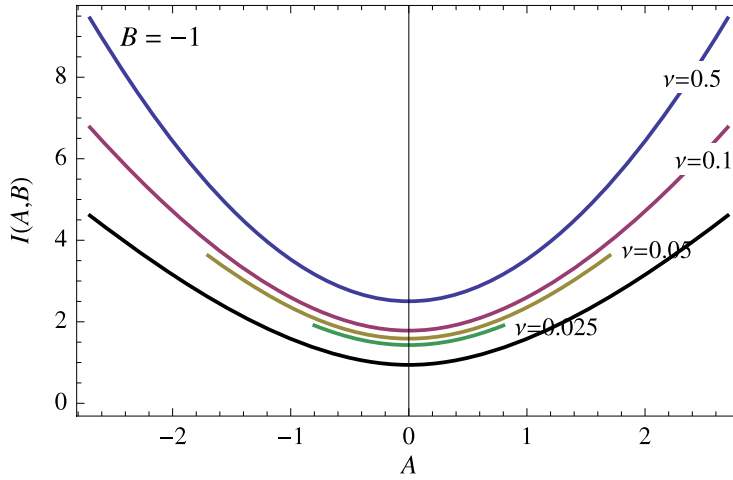


**Figure 8.** Numerical test for  $I(A, B)$  on the line  $B = -1$ .  $\sigma_A = \sigma_B = 1$ . Black line: analytical result for  $I(A, B)$ . Colored lines: rate function  $I(A, B)$  obtained from the numerical integration of the Fokker–Planck equation of the  $AB$  model for different values of  $\nu$ .

Assuming that  $\tilde{\phi}(0, r) > 0$ , we then obtain

$$I(r) = \frac{2\sqrt{2}}{3} r^{3/2} \quad (66)$$

as the solution for  $I$ .<sup>6</sup> In terms of  $A$  and  $B$ , this yields the LDP

$$P(A, B) \approx e^{-I(A, B)/\sqrt{\nu}}, \quad (67)$$

where

$$I(A, B) = \frac{2\sqrt{2}}{3} (A^2 + B^2)^{3/4}. \quad (68)$$

This rate function is different from the one obtained in section 4. This is because the dynamical model studied in section 4 is an approximation of the  $AB$  model in which the dynamics of  $A$  is decoupled from  $B$ . This approximation is not assumed here, so we should take the solution above as a more precise expression of the rate function. The essential point to notice is that both approaches confirm the speed  $1/\sqrt{\nu}$  of the LDP of  $P(A, B)$  near  $\ell_u$ , which also appears to qualitatively match the scaling of the numerical Fokker–Planck results; see figure 8. As before, it is difficult to push the numerical scaling analysis beyond  $\nu = 0.025$ , as the numerical integration of the Fokker–Planck equation becomes unstable for smaller values of  $\nu$ .

## 6. Discussion

The two LDPs that we have derived for  $P(A, B)$  can be thought of as an expansion of  $P(A, B)$  that keeps its two first dominant terms, so that

$$P(A, B) = C_1 e^{-I(A, B)/\sqrt{\nu}} + C_2 e^{-J(A, B)/\nu}. \quad (69)$$

<sup>6</sup> Note that  $I$  must be positive and must vanish on the stable fixed point  $(0, 0)$ .

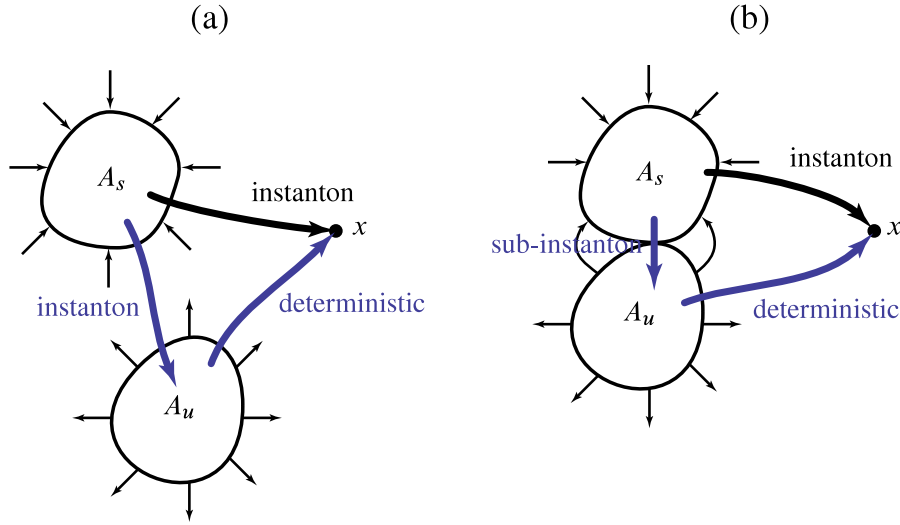


**Figure 9.** (a) Fluctuation paths for disconnected sets of stable ( $A_s$ ) and unstable ( $A_u$ ) fixed points. In this case, any path reaching a point  $x$  must contain an instanton part, even if it goes through  $A_u$  (blue path), so its large deviation probability must have a speed  $1/\nu$ . (b) Fluctuation paths for connected sets of stable and unstable fixed points. In this case, there are fluctuation paths that reach  $x$  via ‘sub-instantons’ (blue path) instead of instantons (black path). Sub-instantons have a large deviation speed smaller than  $1/\nu$ .

As discussed, the dominant term in this expansion is the  $1/\sqrt{\nu}$  term associated with the repelling line and is ‘non-classical’ in the sense that it does not arise from instanton fluctuation paths that are characteristic of the theory of Freidlin and Wentzell [23]. The second term with large deviation speed  $1/\nu$  is the term that arises from this theory: it is associated with instantons emanating from the attracting line and becomes important, for small but finite  $\nu$ , in the vicinity of this line.

The presence of the stable and unstable lines of fixed points is important for obtaining these results, but what is also important is that these two sets of fixed points are connected and that the system can diffuse from one to the other. If the attracting and repelling lines were not connected, then all the fluctuation paths reaching a given point away from these lines would necessarily be instantons having a non-zero action at the  $1/\nu$  order in the exponential of  $P(A, B)$ , which means that  $P(A, B)$  would then globally satisfy an LDP with speed  $1/\nu$ . This is illustrated in a general way in figure 9. There we see that a point  $x$  can be reached from an attracting set  $A_s$  either directly with a single instanton (black path in figure 9(a)), or with a fluctuation path that reaches the repelling set  $A_u$  before reaching  $x$  (blue path). The second part of the latter fluctuation path, going from  $A_u$  to  $x$ , follows the natural dynamics of the system, and so carries zero action, while the first part, going from  $A_s$  to  $A_u$ , is an instanton with non-zero action at the scale  $1/\nu$ . Consequently, the whole path must inherit the action of the instanton, which leads us to conclude that large deviations in this scenario are instanton-related and, thus, have the speed  $1/\nu$ .

If the sets  $A_s$  and  $A_u$  of fixed points are connected, as is the case for the  $AB$  model, then the part of the fluctuation path that goes from the attracting set to the repelling

set (see figure 9(b)) is not an instanton anymore, at least not an instanton with positive action at the scale  $1/\nu$ . In the  $AB$  model, it is a simple diffusing path or sub-instanton that contributes, as we have seen, to a factor  $e^{-c/\sqrt{\nu}}$  in the stationary probability density, where  $c$  is some positive constant. In general, this is larger than the probability of ‘true’ instantons, which scales like  $e^{-c/\nu}$  as  $\nu \rightarrow 0$ . It might be the case that, for points close to the attracting set, and for small but finite values of  $\nu$ , instantons can have a probability greater than the probability of sub-instantons. This happens, for example, in the  $AB$  model near the attracting line. However, the fact is that, because of their lower speed, sub-instantons necessarily have a probability higher than the probability of instantons in the limit  $\nu \rightarrow 0$ , which means that they determine the dominant LDP.

We expect this scenario to apply to more realistic systems having extended and connected sets of steady states. In general, the probability of diffusing paths or sub-instantons going from an attracting set to a repelling set is likely to depend on the particular system considered, but what should be clear is that these paths have, in the low-noise limit, a probability greater than the probability of instantons. As a result, they must determine, if they exist, the dominant large deviation form of the stationary probability density of the system, when such a stationary density exists. In the future, it would be interesting to determine minimal conditions for the appearance of sub-instantons or related fluctuation paths, and to see whether these generally arise in stochastic systems violating detailed balance, as seems to be suggested by our results.

## Acknowledgments

We thank Eric Simonnet for first proposing the study of the  $AB$  model in relation to averaging techniques. We also thank Oleg Zaboronsky and Jason Laurie for interesting discussions. HT acknowledges the hospitality of the Laboratoire de Physique at ENS Lyon, the LPTMC at the Université Paris 6, and the National Institute of Theoretical Physics at the University of Stellenbosch, where parts of this paper were written. The work of FB was supported by the ANR programs STATOCEAN (ANR-09-SYSC-014) and ANR STOSYMAP (ANR-2011-BS01-015). The work of HT was supported by an Interdisciplinary Research Fellowship (RCUK).

## References

- [1] Guckenheimer J and Holmes P, 1983 *Nonlinear Oscillations, Dynamical Systems, and Bifurcations of Vector Fields (Applied Mathematical Sciences vol 42)* (New York: Springer)
- [2] Pego R L and Weinstein M I, *Asymptotic stability of solitary waves*, 1994 *Commun. Math. Phys.* **164** 305
- [3] Bouchet F and Morita H, *Large time behavior and asymptotic stability of the 2D Euler and linearized Euler equations*, 2010 *Physica D* **239** 948
- [4] Mouhot C and Villani C, *On Landau damping*, 2011 *Acta Math.* **207** 29
- [5] Holm D D, Marsden J E, Ratiu T and Weinstein A, *Nonlinear stability of fluid and plasma equilibria*, 1985 *Phys. Rep.* **123** 1
- [6] Morrison P J, *Hamiltonian description of the ideal fluid*, 1998 *Rev. Mod. Phys.* **70** 467
- [7] Arnold V I, *An a priori estimate in the theory of hydrodynamic stability*, 1966 *Izv. Vyssh. Uchebn. Zaved. Mat.* **3**  
Arnold V I, 1969 *Am. Math. Soc.* **19** 267 (Engl. transl.)
- [8] Bouchet F and Venaille A, *Statistical mechanics of two-dimensional and geophysical flows*, 2012 *Phys. Rep.* **515** 227
- [9] Touchette H, *The large deviation approach to statistical mechanics*, 2009 *Phys. Rep.* **478** 1
- [10] Sommeria J, *Two-dimensional turbulence*, 2001 *New Trends in Turbulence (Les Houches Summer School vol 74)* (New York: Springer) pp 385–447

- [11] Tabeling P, *Two-dimensional turbulence: a physicist approach*, 2002 *Phys. Rep.* **362** 1
- [12] Schneider K and Farge M, *Final states of decaying 2D turbulence in bounded domains: influence of the geometry*, 2008 *Physica D* **237** 2228
- [13] Robert R and Sommeria J, *Statistical equilibrium states for two-dimensional flows*, 1991 *J. Fluid Mech.* **229** 291
- [14] Miller J, *Statistical mechanics of Euler equations in two dimensions*, 1990 *Phys. Rev. Lett.* **65** 2137
- [15] Bouchet F and Sommeria J, *Emergence of intense jets and Jupiter's Great Red Spot as maximum-entropy structures*, 2002 *J. Fluid Mech.* **464** 165
- [16] van Kampen N G, 1992 *Stochastic Processes in Physics and Chemistry* (Amsterdam: North-Holland)
- [17] Graham R, *Macroscopic potentials, bifurcations and noise in dissipative systems*, 1989 *Noise in Nonlinear Dynamical Systems* vol 1, ed F Moss and P V E McClintock (Cambridge: Cambridge University Press) pp 225–78
- [18] Moss F and McClintock P V E (ed), 1989 *Noise in Nonlinear Dynamical Systems* vol 1 (Cambridge: Cambridge University Press)
- [19] Mannella R and McClintock P V E, *Noise in nonlinear dynamical systems*, 1990 *Contemp. Phys.* **31** 179
- [20] Dykman M I and Lindenberg K, *Fluctuations in nonlinear systems driven by colored noise*, 1994 *Contemporary Problems in Statistical Physics* ed G H Weiss (Philadelphia: SIAM) pp 41–101
- [21] Luchinsky D G and McClintock P V E, *Irreversibility of classical fluctuations studied in analogue electrical circuits*, 1997 *Nature* **389** 463
- [22] Luchinsky D G, McClintock P V E and Dykman M I, *Analogue studies of nonlinear systems*, 1998 *Rep. Prog. Phys.* **61** 889
- [23] Freidlin M I and Wentzell A D, 1984 *Random Perturbations of Dynamical Systems* (Grundlehren der Mathematischen Wissenschaften vol 260) (New York: Springer)
- [24] Berglund N and Gentz B, *Anomalous behavior of the Kramers rate at bifurcations in classical field theories*, 2009 *J. Phys. A: Math. Theor.* **42** 052001
- [25] Berglund N and Gentz B, *The Eyring–Kramers law for potentials with nonquadratic saddles*, 2010 *Markov Proc. Rel. Fields* **16** 549
- [26] Graham R, *Fluctuations in the steady state*, 1995 *25 Years of Non-Equilibrium Statistical Mechanics* ed J J Brey, J Marro, J M Rubí and M S Miguel (New York: Springer) pp 125–34